Hindawi
Mathematical Problems in Engineering
Volume 2024, Article ID 2786501, 19 pages
https://doi.org/10.1155/2024/2786501

Research Article

Influence of Structural Parameters of Gearbox Seal System of Electrical Multiple Units on Seal Performance

Longjiang Shen,[1] **Yingmou Zhu**,[1] **Shuai Shao**,[2] **and Chengyu Sha**[2]

[1]*State Key Laboratory of Heavy-Duty and Express High-Power Electric Locomotive, CRRC Zhuzhou Locomotive Co., Ltd., Zhuzhou 412001, China*
[2]*State Key Laboratory of Rail Transit Vehicle System, Southwest Jiaotong University, Chengdu 610031, China*

Correspondence should be addressed to Shuai Shao; swjtushaoshuai@163.com

Received 8 March 2023; Revised 6 April 2024; Accepted 17 April 2024; Published 7 May 2024

Academic Editor: Taoreed Owolabi

Copyright © 2024 Longjiang Shen et al. This is an open access article distributed under the Creative Commons Attribution License, which permits unrestricted use, distribution, and reproduction in any medium, provided the original work is properly cited.

The gearbox seal system is a critical component of the electrical multiple units drive system, with a direct impact on the safety and reliability of train operations. This study intends to analyze how structural parameters of the gearbox seal system influence the seal performance from the viewpoint of "oil–air separation and scavenge oil" by using a discrete phase model and volume of fluid. The results show that the oil–air separation performance is mainly affected by the oil droplets' inertia force and the airflow traction force, and the scavenge oil performance is decided by the oil–air separation performance of each seal chamber. The relationships between seal chamber size, axial seal clearance width, height difference, scavenge oil hole diameter, and seal performance are analyzed, and the study also found that optimizing the stator chamber depth–width ratio of the seal system studied in this paper at 2.5, reducing the rotor chamber depth–width ratio and axial seal clearance width, and increasing the relative height difference can improve the seal performance. And increasing the scavenge oil hole diameter also enhances the seal system's performance. The simulation results can be used as design references for gearbox seal systems.

1. Introduction

The gearbox of electrical multiple units (EMU) often operates under severe working conditions such as frigidity, high temperature, and humidity. The reliability of its seal system is the premise of the safe operation of the gearbox. Commonly used seal forms of EMU gearbox can be divided into contact seal, noncontact seal, and combined seal. The contact seal and the combined seal need to use rubber seal rings. Rubber seal rings are indispensable for contact seal and combination seal. However, during subsequent use of seals, the rubber seal ring may cause fretting corrosion due to wear or heat cracking due to high friction. Therefore, compared with contact seals and combined seals, the noncontact seals have better durability.

The noncontact seal used in the EMU gearbox is comprised of a labyrinth seal located at the shaft end and a scavenge oil structure. Scholars around the world have conducted extensive research on the sealing and leakage mechanism of labyrinth seals. Zhang et al. [1, 2], Wu and San Andrés [3], and Andrés et al. [4] studied the seal mechanism, leakage characteristics, and influencing factors of straight-through labyrinth seal, stepped labyrinth seal, and interlocked labyrinth seal. The results demonstrated that the interlocked labyrinth seal is the most effective at sealing. Under working conditions with an inlet pressure of 6.9 bar, outlet pressure of 5.5 bar, and rotor speed of 10,000 rpm, its sealing effectiveness is approximately 21% higher than that of a stepped seal with a similar-sized structure. Decreasing the gap between the rotor and the stator can enhance the effectiveness of the seal; however, excessive clearance reduction can cause seal tooth bending and mushroom deformation. Yan et al. [5] conducted a study on the leakage characteristics of the labyrinth seal, examining the impact of the bending angle of the seal teeth and the mushroom radius on the seal's performance. From the viewpoint of energy dissipation, Haghiabi et al. [6] and Wang et al. [7] studied the energy variation of the fluid medium before and after flowing through the labyrinth weir. Through the above literature, we can see that when the sealing medium flows

through the seal chamber and the seal clearance, its kinetic energy will be converted at the throttling clearance and dissipated in the expansion cavity, so the leakage can be reduced.

The sealing mediums used in [1–7] are all ideal gas, but it is quite different from the actual situation inside the gearbox. As a gearbox rotates at high speeds, it is filled with a combination of lubricant and air, which helps to maintain the smooth rotation of gears. Using a single-phase air that obeys the ideal gas law to analyze the seal characteristic of the seal system is obviously unable to meet the requirements. To address this issue, He et al. [8] explored the effect of the seal tooth clearance on the leakage of staggered labyrinth seals, using a gas–fluid two-phase mixture as the working medium. The findings revealed that the labyrinth seal leaked the least when the seal clearance was between 0.5 and 1 mm. Zhang and Childs [9] used an annular seal test system to see how much a long labyrinth seal leaked when it was working in a wet gas environment. The findings demonstrated that there was a correlation between the volume fraction of the liquid phase in the inlet mixed medium and the rate of leakage, which showed a steady increase. According to research by Li et al. [10], who looked at how wet gas conditions affected the seal performance of the annular seal of the turbomachinery, overall leakage of the mixed medium rose with an increase in the volume percentage of the liquid phase in the wet gas, while leakage of the gas phase decreased. These results also demonstrated that using an ideal gas as the working medium is inappropriate for investigating the gearbox seal system's seal characteristics.

Although reducing leakage flow is the main function of the gearbox seal system, the scavenge oil performance of the gearbox seal system should also receive more attention. Farall et al. [11, 12] mixed lubricating oil in the form of discrete phase droplets in the airflow, thought about how oil droplets and oil film interact and how oil film moves, and then numerically simulated the flow law of oil film in the bearing chamber. The findings indicated that the oil film thickness and motion law on the bearing chamber wall would be affected by modifying the boundary conditions of the scavenge port and vent port. In addition, Zhang et al. [13, 14] analyzed the oil–gas separation characteristics of the gearbox seal system under various operating conditions (oil droplet diameter, outlet pressure) and geometric parameters (axial gap width, axial gap height difference, radial seal tooth angle, radial seal meshing ratio) using the discrete phase model (DPM) and the oil droplet–wall collision model. However, the scavenge oil process after the separation of the mixed medium was not investigated in their research. Therefore, it is unclear how the structural features of the seal system impact oil–gas separation and scavenge oil characteristics and mechanisms.

This paper presented a numerical method for analyzing the oil–air separation and scavenge oil performance of the EMU gearbox seal system. In the established numerical model, it is considered that the seal performance of the gearbox seal system is jointly determined by the oil–air separation performance and scavenge oil performance after separation. Correspondingly, the leakage of the seal system is also composed of lubricating oil that has not achieved oil–air separation and lubricating oil that has achieved separation but fails to achieve effective scavenge oil. The DPM is used to analyze the oil–air separation performance, and the volume of fluid (VOF) is used to analyze the scavenge oil performance after separation. To improve the calculation accuracy, the interaction between oil droplets and the seal chamber's wall is considered in the DPM. Additionally, based on the established numerical model, numerical simulations were conducted to investigate the impact of structural parameters on the seal performance of the gearbox seal system. The oil–air separation performance mainly depends on the inertial force on the droplets and the drag force of the airflow, while the scavenge oil performance depends on the oil–air separation effectiveness of each seal chamber. The optimal depth–width ratio of the stator chamber seal system studied in this paper is 2.5. Decreasing the depth–width ratio of the rotor chamber and the axial seal clearance, and increasing the relative height difference can enhance the seal performance of the seal system.

2. Numerical Methods

2.1. Two-Phase Flow Model. While the EMU is running at high speed, the oil at the bottom of the box is stirred up by the gear, broken into tiny droplets by the action of the tooth surface and the box wall, and combined with the air to produce an oil–air mixture. Because of this, the performance of the seal system has to be assessed using a two-phase flow model. The oil–air mixture needs to satisfy the basic equations of fluid motion during the flow process, namely, the continuity equation, momentum conservation equation, and energy conservation equation. Its general form is [15] as follows:

$$\frac{\partial(\rho\phi)}{\partial t} + \nabla(\rho \boldsymbol{u}\phi) = \nabla\left(\Gamma_\phi \nabla\phi\right) + S_\phi, \tag{1}$$

where ϕ is a general variable; t is the time; $\boldsymbol{u}$ is the velocity vector; Γ_ϕ is the diffusion coefficient; ρ is the fluid density; S_ϕ is the source term.

One of the steps in analyzing the oil–air mixture in the gearbox seal system is to trace the trajectory of the tiny droplets of lubricating oil. This mixture medium typically enters the seal chamber through the inlet of the seal system. The volume fraction of lubricating oil in the air is usually less than 10%, making it suitable for analysis using the DPM. To assess the oil–air separation characteristics, the DPM is used to derive the trajectory of discrete phase particles in the flow field. This is achieved by solving the differential equation of particle force in the Lagrangian coordinate system. When taking into consideration a single particle, the force balance equation may be written as follows [16]:

$$\frac{du_d}{dt} = F_D(u_c - u_d) + \frac{g(\rho_d - \rho_c)}{\rho_d} + F_x, \tag{2}$$

$$F_D = \frac{18\mu_c}{\rho_d d_d^2}\frac{C_D Re_d}{24}, \tag{3}$$

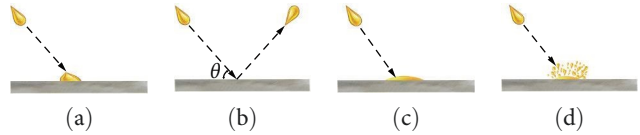

Figure 1: Schematic diagram of collision between oil droplets and wall surface: (a) stick; (b) rebound; (c) spread; (d) splash.

$$Re_d = \frac{\rho d_d |u_c - u_d|}{u_c}, \tag{4}$$

$$C_D = \alpha_1 + \frac{\alpha_2}{Re_d} + \frac{\alpha_3}{Re_d'}, \tag{5}$$

where F_D is the drag force per unit discrete phase mass; u_c is the continuous phase velocity; u_d is the discrete phase velocity; μ_c is the continuous phase hydrodynamic viscosity; ρ_c is the continuous phase density; ρ_d is the discrete phase density; d_d is the discrete phase diameter; C_D is the drag coefficient; Re_d is the discrete phase Reynolds number; α_1, α_2 and α_3 are the constants; g is the acceleration of gravity; F_x is the additional force on a single particle.

After the oil–air separation is realized, the oil droplets will no longer be mixed with air and will instead create a film on the seal chamber wall. Simultaneously, it is assumed that the lubricating oil and air have the same velocity and pressure field and that the oil–air two-phase flow can be characterized using the same equations as a single-phase flow. To evaluate the scavenge oil process, the VOF model is applied, which can simulate two or more nonmiscible fluids by solving an independent momentum equation and calculating the volume fraction of each fluid as it flows through the domain. The cross-sectional area between phases is tracked in the VOF model by solving the continuity equation for the volume fraction of a single or multiphase, and the equation for the qth phase can be expressed as follows:

$$\frac{\partial \alpha_q}{\partial t} + v_q \cdot \nabla \alpha_q = \frac{S_{\alpha_q}}{\rho_q}, \tag{6}$$

where α_q is the volume fraction of the qth phase, v_q is the velocity of the qth phase, and $S\alpha_q$ is the source term of the qth phase, which defaults to 0. ρ_q is the density of the qth phase.

Since the gearbox seal system only involves two phases, lubricating oil and air, the sum of volume fractions of all phases in each control unit of the VOF model equals 1; that is, Equation (6) is simplified as follows:

$$\alpha_{\text{air}} + \alpha_{\text{oil}} = 1, \tag{7}$$

where α_{air} is the volume fraction of air; α_{oil} is the volume fraction of lubricating oil. When $\alpha_{\text{air}} = 0$, the control volume is filled with lubricating oil; when $\alpha_{\text{air}} = 1$, there is no lubricating oil in the control volume; when $0 < \alpha_{\text{air}} < 1$, there is air and lubricating oil in the control volume.

2.2. Droplet–Wall Interaction Model. The pressure differential between the inlet and outlet forces the mixing medium to flow in the seal chamber. The state and energy of the oil droplets will be altered before and after collision with the wall surface. As illustrated in Figure 1, the states of oil droplets after collision with a wall may be classified as stick, rebound, spread, and splash, depending on the incidence angle and velocity of the oil droplets. Stick and spread may be thought of as oil droplets that achieve oil–air separation because they are considered to be caught by the seal chamber's wall surface. The rebound and splash oil droplets are oil droplets that continue to participate in subsequent motions until they are separated by the seal chamber's wall surface or escape via the outlet.

Table 1: The droplet state after collision with a humid wall [13, 14].

Oil droplet state	Critical Weber number Wec
Stick → rebound	$Wec \approx 1$
Rebound → spread	$Wec \approx 5$
Spread → splash	$Wec = 1{,}320 \times \text{La}^{-0.18}$

The collision of oil droplets with the wall in the gearbox seal system can be classified as either drywall or humid wall collisions, depending on the wall's condition. When an oil droplet collides with the wall surface of the seal chamber, it causes the previously drywall to become humid. For this reason, all of the seal chamber's walls can be considered humid walls for evaluating the seal system's performance. It is almost unlikely for an oil droplet to splash after impacting a wall in the gearbox seal system [13]. Consequently, when an oil droplet impacts the wall of the seal chamber, it can be in one of three states: stick, rebound, or spread. The states of the droplet in the high-speed airflow after collision with the wall are strongly connected to the Weber number We and the Laplace number La [17]. The We and La are usually used to evaluate the state of the droplet after the collision, which are determined by Equations (8) and (9), respectively. The relationship between We and the droplet state after collision is shown in Table 1.

$$We = \frac{\rho_o V_n^2 d_o}{\sigma_o}, \tag{8}$$

$$La = \frac{\rho_o \sigma_o d_o}{\mu_o^2}, \tag{9}$$

where ρ_o is the oil droplet density, d_o is the oil droplet diameter, μ_o is the oil droplet viscosity, σ_o is the oil droplet surface tension, and V_n is the normal collision velocity of the oil droplet.

2.3. Turbulence Model. During gearbox operation, the oil–air mixture medium is characterized by obvious turbulent flow due to the high-speed rotating seal ring. The renormalization group (RNG) k–ε turbulence model is better equipped to handle high strain rates and large streamline bend flows, taking into account the rotation and rotational flow in the average flow and the effect of the separated flow vortex. As a result, it is more suitable for numerical flow field analysis of seal systems with high-speed rotating seal rings. Given these considerations, the RNG k–ε turbulence model was selected to simulate the flow field of the gearbox seal system, and its governing equation is as follows [18]:

$$\frac{\partial(\rho k)}{\partial t}+\frac{\partial(\rho\varepsilon u_i)}{\partial x_i}=\frac{\partial}{\partial x_j}\left[\alpha_k\mu_{\text{eff}}\frac{\partial k}{\partial x_j}\right]+G_k+\rho\varepsilon, \tag{10}$$

$$\frac{\partial(\rho\varepsilon)}{\partial t}+\frac{\partial(\rho\varepsilon u_i)}{\partial x_i}=\frac{\partial}{\partial x_j}\left[\alpha_\varepsilon\mu_{\text{eff}}\frac{\partial\varepsilon}{\partial x_j}\right]+\frac{C_{1\varepsilon}^{*}\varepsilon}{k}G_k-C_{2\varepsilon}\rho\frac{\varepsilon^2}{k}, \tag{11}$$

where ρ is the fluid density, k is turbulent kinetic energy, ε is dissipation rate, t is time, i and j are tensor indexes, x_i and u_i are displacement and velocity respectively, a_k and a_ε are the reciprocal of the effective turbulent Prandtl number of turbulent kinetic energy k and dissipation rate ε, respectively, μ_{eff} is the correction term of turbulence model to turbulent viscosity, which is the turbulent kinetic energy term generated by average velocity gradient, $C_{1\varepsilon}^{*}$ is the correction coefficient of RNG k–ε turbulence model constant $C_{1\varepsilon}$, and the remaining terms are model constants.

3. Model and Simulation Conditions

3.1. Geometric Model. The seal system of the EMU gearbox includes an annular labyrinth seal, and a two-stage scavenge oil structure, as illustrated in Figure 2. The annular labyrinth seal consists of an axial bilateral straight-through labyrinth seal and a radial plug-in labyrinth seal. By setting seal teeth on the rotating seal ring and shaft end bushing from the inlet to the outlet, three groups of seal chambers are set in the axial seal, which are respectively marked as chamber *I*, chamber *II*, and chamber *III*, respectively. Each group of chambers includes a stator chamber and a rotor chamber. In order to raise the flow resistance within the limited space and improve the oil–air separation effectiveness, a radial plug-in labyrinth seal is set between chamber *III* and the outlet.

The two-stage scavenge oil structure is located below the annular labyrinth seal. The scavenge oil structure has two purposes. First, it creates a difference in pressure between the scavenge port and the labyrinth seal, which affects how the pressure is distributed in the labyrinth seal. Second, the oil droplets collide with the seal chamber's wall, separating a portion of the oil droplets from the oil–air mixture and this separated oil is directed back to the gearbox via the scavenge oil port, facilitated by the force of gravity and the pressure gradient between the labyrinth seal and scavenge port. This process ensures effective scavenge oil. However, some oil droplets that do not collide with the chamber wall, or those that are trapped but fail to achieve effective scavenge oil, eventually leak out through the outlet.

3.2. Boundary Conditions. When the seal system is running stably, the flow in the seal chamber can be regarded as fully developed turbulence, which is calculated according to the 3D steady flow model. To define the seal system's inlet pressure and scavenge port pressure, the numerical outcomes of the gearbox's flow field within the gearbox are adopted and set as 580 and 240 Pa, respectively. Meanwhile, the outlet pressure is taken as an environment back pressure value of −600 Pa [13, 14]. The operating pressure during the simulation process is defined as 101,325 Pa. Lubricating oil 75−90 W is used to define the physical properties of oil droplets.

When analyzing the separation effectiveness of the seal system, the DPM is adopted, with air as the continuous phase and lubricating oil droplets as the discrete phase. The escape boundary is used for the seal system's inlet, outlet, and scavenge port, whereby oil droplets that reach the boundary are considered to escape from the system and are no longer included in the subsequent calculations. To define the seal chamber wall, a user-defined program called DEFINE_DPM_BC is developed in Ansys Fluent 17.0 (ANSYS, Inc., Canonsburg, PA, USA), following the guidelines provided in Table 1. When the *We* of an oil droplet falls within the range of $1 < We < 5$, it collides against the wall and rebounds, with the trajectory thereafter determined by Equations (12) and (13) [19]. When the *We* of oil droplets is $We < 1$ or $We > 5$, the oil droplets will collide with the wall and adhere to the wall. These oil droplets are recorded as traps and no longer participate in subsequent calculations.

$$e_n = 0.993 - 0.176\theta - 1.56\theta^2 - 0.49\theta^3, \tag{12}$$

$$e_\tau = 0.988 - 0.166\theta + 2.11\theta^2 - 0.67\theta^3, \tag{13}$$

where e_n and e_τ represent the normal and tangential rebound coefficients, respectively, θ represents the angle of incidence.

The quality of lubricating oil that leaks from the gearbox seal system m_{e} consists of two components: lubricating oil quality that leaked without oil–air separation m_{e1} and lubricating oil quality that achieved oil–air separation but lacked adequate scavenging oil m_{e2}. The seal characteristic of the seal system depends on the separation characteristic of the oil–air mixture and the scavenge oil performance after separation.

The effectiveness of oil–air separation of the seal system η_{sep} can be evaluated using Equation (14):

$$\eta_{\text{sep}} = \left(1-\frac{m_{\text{e1}}}{m_{\text{in}}}\right)\times 100\%, \tag{14}$$

where m_{in} denotes the total mass of oil droplets that enter the seal system.

The effectiveness of scavenge oil of the seal system η_{sca} can be evaluated using Equation (15):

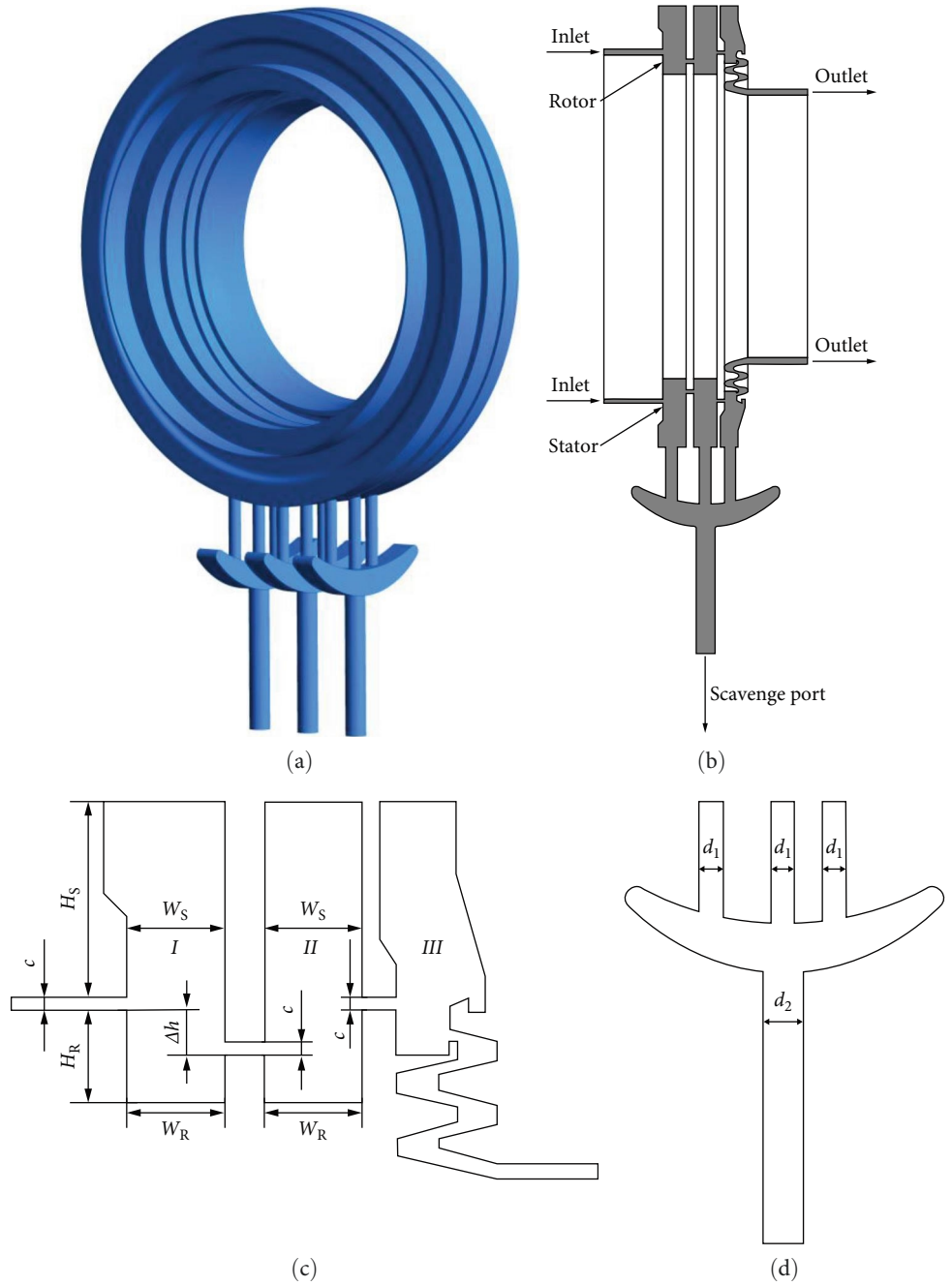

FIGURE 2: Schematic diagram of seal system: (a) 3D schematic diagram; (b) half-cutaway view; (c) labyrinth seal; (d) scavenge oil structure.

$$\eta_{sca} = \left(1 - \frac{m_{e2}}{m_{in} - m_{e1}}\right) \times 100\%. \tag{15}$$

The amount of lubricating oil that leaks from the gearbox seal system m_e is calculated by Equation (16):

$$m_e = m_{e1} + m_{e2}. \tag{16}$$

The sealing effectiveness of seal system η_{seal} is calculated by Equation (17):

$$\eta_{seal} = \left(1 - \frac{m_e}{m_{in}}\right) \times 100\%. \tag{17}$$

3.3. Mesh Sensitivity Analysis. The density and quality of mesh have an important influence on the accuracy and effectiveness of numerical simulation. The gearbox seal system is divided into unstructured grids, with internal nodes selected as the node type. The wall surface adopts standard wall functions, and key areas such as seal clearances are locally refined. To test mesh sensitivity, six different meshes were analyzed

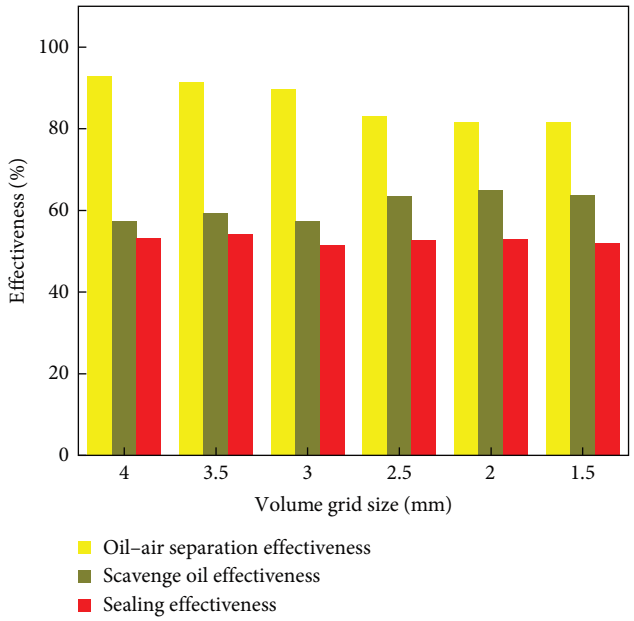

FIGURE 3: The relationship between the effectiveness and the volume grid size.

under rated gearbox conditions, with oil–air separation effectiveness, scavenge oil effectiveness, and sealing effectiveness serving as parameters. Select a tetrahedral grid with a mesh size of 2–4 mm to partition the computational domain, with a corresponding number of grid elements ranging from 0.773 to 1.596 million. As shown in Figure 3, reducing the volume mesh size resulted in decreasing oil–air separation effectiveness and increasing scavenge oil effectiveness. However, the volume mesh size had little effect on sealing effectiveness, which tended to stabilize at smaller mesh sizes. After balancing simulation accuracy and computational time, a tetrahedral mesh with a size of 2.5 mm was chosen to discretize the computational domain. A tetrahedral mesh with a size of 1 mm was used for local refinement in the inlet, seal clearances, and scavenge oil structure. The resulting number of mesh cells was 1,016,682, with 245,389 nodes. This mesh was then used for subsequent numerical simulations.

4. Experimental Validations

The structural model of the oil–gas separator, as well as the physical parameters of the lubricating oil, can be found in [20], which was applied to compare and prove the accurateness and applicability of the simulation method for the seal characteristics of the gearbox seal system presented in this paper. The experimental process of the gas engine labyrinth oil–gas separator is illustrated in Figure 4, where blow-by gas directly enters the separator after coming out of the crankcase. The oil that is not separated is collected by oil–gas collection tooling *I* and recorded as m_1, while the separated oil is collected by oil–gas collection tooling *II* and recorded as m_2. The mass difference between oil–gas collection tooling *I* and oil–gas collection tooling *II* before and after the experiment represents the up oil quantity and return oil quantity, respectively. The oil–gas separation effectiveness is defined as

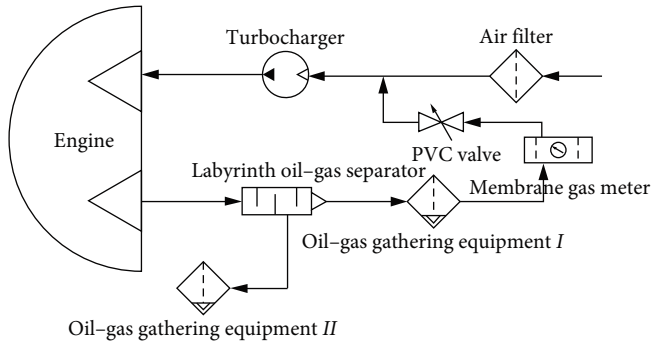

FIGURE 4: Experimental process of gas engine labyrinth oil–gas separator.

the ratio of oil return quantity to the total oil quantity, where the total oil quantity is the sum of up oil quantity and return oil quantity, and the separation effectiveness of oil–gas separator is calculated according to Equation (18).

$$\eta = \left(\frac{m_2}{m_1 + m_2}\right). \tag{18}$$

By keeping the throttle fully open, which means operating the engine under full load, and the blow-by gas during the experimental process is kept constant. Then, the up oil quantity and the return oil quantity in the oil–gas collection tooling *I* and *II* are, respectively, measured and recorded every 10 min for a duration of 1 hr. The measured values are then weighted averaged. Table 2 compares the separation effectiveness of oil–gas separator obtained by numerical simulation and experimental bench at different blow-by flows. From Table 2, it can be observed that with an increase in the crankcase blow-by gas, the up oil quantity changes minimally, while the return oil quantity increases significantly, resulting in a continuous increase in the separation effectiveness. Both numerical simulation results and experiment bench results show that the separation effectiveness reaches over 80% at different blow-by gas, indicating that the oil–gas separator effectively separates oil and gas in the blow-by gas. Although the numerical simulation values are slightly higher than the experimental values at each blow-by gas, the overall trend is consistent, and the error range is less than 5%, indicating that the numerical method used is reliable. The higher simulation values compared to experiment values may be due to the simplification of the force acting on oil droplets in the simulation without considering factors such as collision, fusion, and breakup among oil droplets.

5. Results and Discussion

5.1. Analysis of Seal Mechanism. The continuous phase air affects how the lubricating oil droplets move inside the seal system, and the distribution of lubricating oil after separation, in turn, affects the airflow field. Seal system boundary conditions are defined according to the research results of Zhang et al. [13, 14]. With pressure boundary conditions, the

Table 2: Separation effectiveness of oil–gas separator.

Blow-by gas (L/min)	Experiment bench			Numerical simulation		
	Up oil quantity (g)	Return oil quantity (g)	Separation effectiveness (%)	Up oil quantity (g)	Return oil quantity (g)	Separation effectiveness (%)
100	2.1	8.3	79.8	1.9	8.82	82.3
122	2.4	12	83.3	2.1	11.4	84.4
179	3.9	25.4	86.7	3.8	26.9	87.6

inlet, outlet, and scavenge ports are defined as 580, −600, and 240 Pa, respectively. The rotor chamber operates at a speed of 2,000 rpm, and the oil–air mixture medium contains a volume fraction of lubricating oil of 7.72%. By analyzing the oil–air separation process and scavenge oil process of the seal system on the oil–air mixture composed of 5 μm diameter oil droplets, the sealing mechanism of the seal system is further revealed, as shown in Figures 5 and 6.

It can be seen from Figures 5(a) and 5(b) that during the oil–air separation process, the oil–air mixture enters at a high speed from the inlet, and the pressure of each seal chamber gradually decreases along the flow direction. After passing through the seal clearance, the flow direction of the mixed medium changes, and an obvious vortex is formed in the seal chamber. Due to the inevitable frictional resistance between the oil–air mixture and the wall of the seal chamber, the kinetic energy of the oil–air mixture is finally converted into frictional heat energy, which realizes the sealing and reduces the leakage.

As shown in Figure 5(c), under the action of the rotor chamber, oil droplets are affected by the airflow and enter the seal system in a rotating state. A small portion of the oil droplets, under the entrainment effect of the straight-through airflow, directly escape from the seal outlet without colliding with the wall, escape from the outlet without colliding with the wall under the direct airflow, resulting in the m_{e1} and reducing the η_{sep}. Due to the existence of clearance and cavity vortex flow in the sealing structure, most oil droplets are injected into the seal chamber at high speed with the airflow. Under the action of cavity vortices, the oil droplets are subjected to centrifugal force, and their motion state changes, causing them to detach from the straight-through airflow and enter the seal chamber, colliding with the wall surface to achieve oil–air separation. Therefore, the oil droplets in the seal system are subjected to the drag effect of straight-through airflow and the centrifugal effect of the vortex. The stronger the drag effect of the airflow, the easier it is for oil droplets to be trapped and moved by the airflow. The stronger the vortex centrifugal effect, the easier it is for oil droplets to achieve oil–air separation from the oil–air mixture. The combined effects of airflow drag and vortex centrifugation determine the motion trajectory of the oil droplets and affect the separation effectiveness and seal performance of the seal system.

Figure 6 shows the pressure and velocity nephogram during the scavenge oil process. Compared with the separation process, the pressure of seal chamber *III* is the highest, followed by that of seal chamber *II*, and the pressure of seal chamber *I* is the lowest. Combining with Figure 5(d), it can be seen that the oil-separation effectiveness of seal chamber *III* is the highest. This is mainly because a radial seal is set at the rear of seal chamber *III*, which significantly weakens the straight-through effect of the sealing medium and results in a large number of oil droplets being separated in chamber *III*. Additionally, due to the pressure gradient between the inlet and outlet, the separated lubricating oil in chambers *I* and *II* will also flow to chamber *III* through the seal clearance. Therefore, the pressure of chamber *III* is the highest, and the pressure of chamber *II* is higher than that of chamber *I*. Affected by the pressure distribution of the continuous phase air, the lubricating oil will still form vortices in the seal chambers *I* and *II* during the scavenge oil process, and its position is consistent with the position of the vortex in the oil–air separation process. Most of the successfully separated lubricating oil is directly returned to the gearbox through the scavenge port. However, there is still a portion of separated lubricating oil that escapes from the outlet along the radial seal.

The mass flow rate of the scavenge oil port in the scavenge oil process of the seal system is taken as the effective scavenge oil quantity, and the outlet mass flow rate is taken as m_{e2}, and the η_{sca} can be obtained. Combined with the oil–air separation process and scavenge oil process, the seal performance of the seal system is comprehensively analyzed. Figure 7 shows the sealing effectiveness and lubricating oil distribution of the seal system. From the diagram, it can be seen that theη_{seal} is determined by the η_{sep} and the η_{sca}, and the m_e is composed of m_{e1} and m_{e2}.

5.2. Influence of Seal Chamber Size. The space volume of the vortex formed by the oil–air mixture in the stator cavities of different structures is different, which will lead to different η_{sep} and η_{sca}. The relation between the depth–width ratio and η_{seal} of oil droplets with different diameters is depicted in Figure 8(a). It is possible to demonstrate that increasing the depth–width ratio of the stator seal chamber has the same η_{seal} change trend for oil droplets of different diameters, which raises first and then descends. When the depth–width ratio is 2.5, the η_{seal} is the highest. The relationship between the η_{sep}, η_{sca}, and η_{seal} of oil droplets with the medium diameter and the depth–width ratio of the stator chamber is illustrated in Figure 8(b). As the depth–width ratio of the stator chamber rises, the η_{sep} raises first and then descends; the change trend of η_{sca} is not obvious, and when the depth–width ratio is 2.5, the η_{sep} is the highest.

The air of the oil–air mixture forms vortexes in the stator chamber, which makes the movement of the oil droplets more complicated. The vortex increases the probability of collision between the oil droplets and the wall and improves the η_{sep}. As shown in Figure 9, the depth–width ratio of the

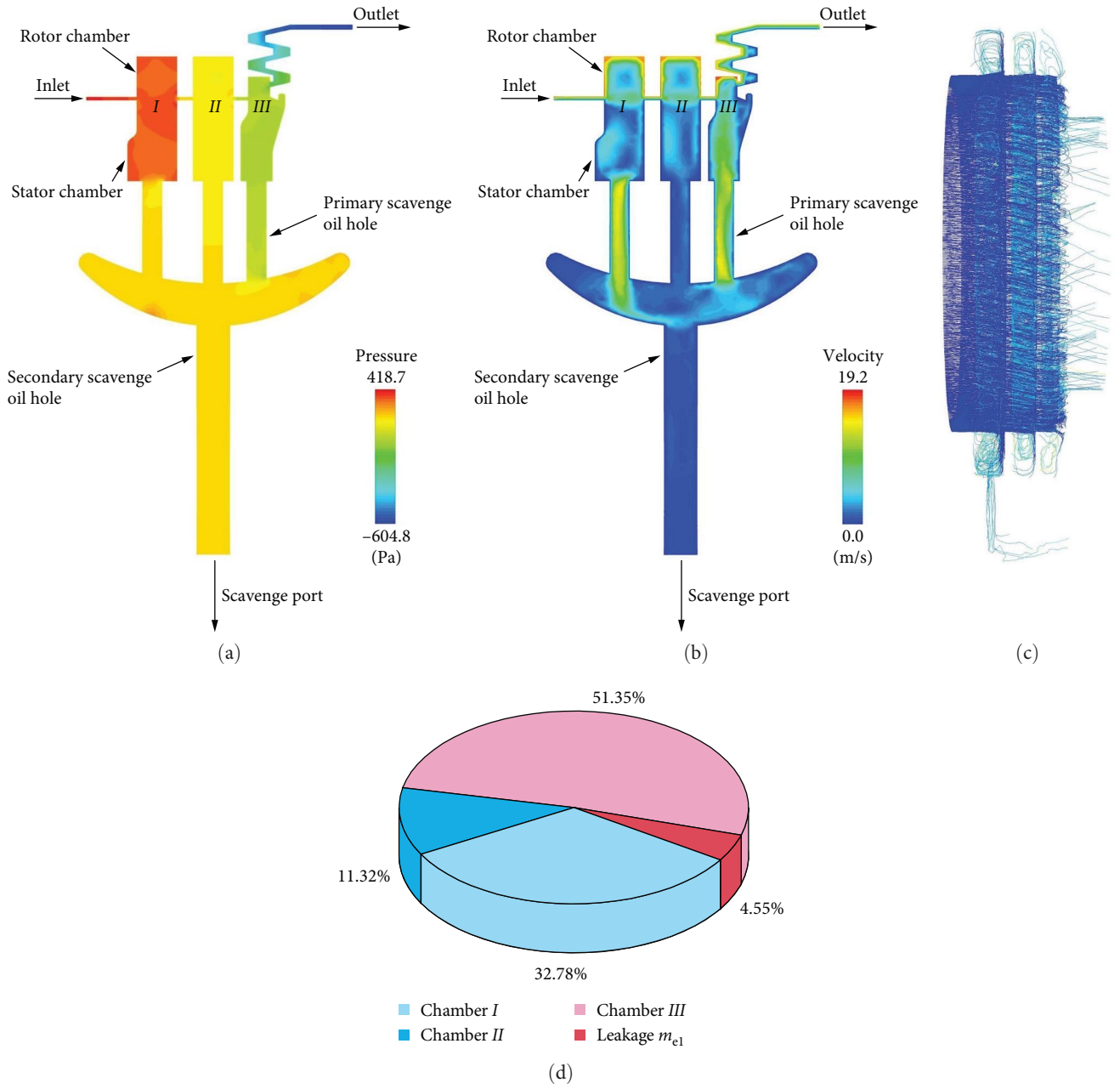

FIGURE 5: Flow field characteristics of the separation process in seal systems: (a) the pressure cloud nephogram of the separation process; (b) the velocity cloud nephogram of the separation process; (c) the oil droplet trajectory; (d) oil–air separation effectiveness of each seal chamber.

stator chamber will affect the formation of the vortex. When the depth–width ratio of the stator chamber is small, as the depth–width ratio increases, the volume of the seal chamber increases, and the airflow gradually forms an effective vortex in the seal chamber. Under the action of eddy current, the centrifugal force of the oil droplets entering the seal chamber increases, so that they can get rid of the drag effect of the airflow and increase the probability of collision with the wall. At the same time, the chamber volume increases, which increases the effective wall area where the oil droplets collide with the wall surface and also promotes the η_{sep}. When the depth–width ratio of the stator chamber is further increased, the effective eddy current cannot be formed in the upper region of the chamber due to the chamber width, resulting in the actual eddy current region in the stator chamber basically unchanged, as shown in Figure 9(e). Due to the limited volume of the vortex, when the depth–width ratio of the stator chamber continues to increase, the vortex does not contact with the upper end, resulting in a decrease in the effective collision area, which reduces the η_{sep}.

The lubricating oil that realizes oil–air separation flows back to the bottom of the seal system along the stator chamber wall surface, and the effective scavenge oil is realized. The η_{sca} depends on the η_{sep}. Figure 10 shows the oil–air

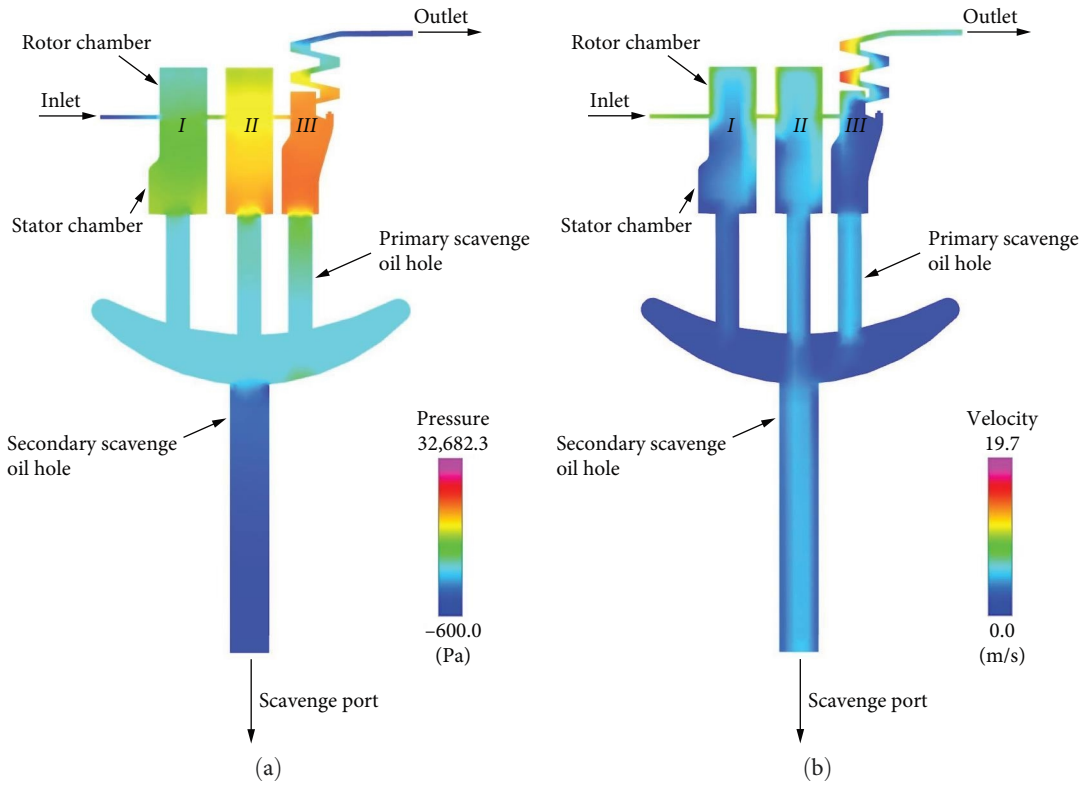

Figure 6: Flow field characteristics of scavenge oil process in seal systems: (a) the pressure cloud nephogram of the scavenge oil process; (b) the velocity cloud nephogram of the scavenge oil process.

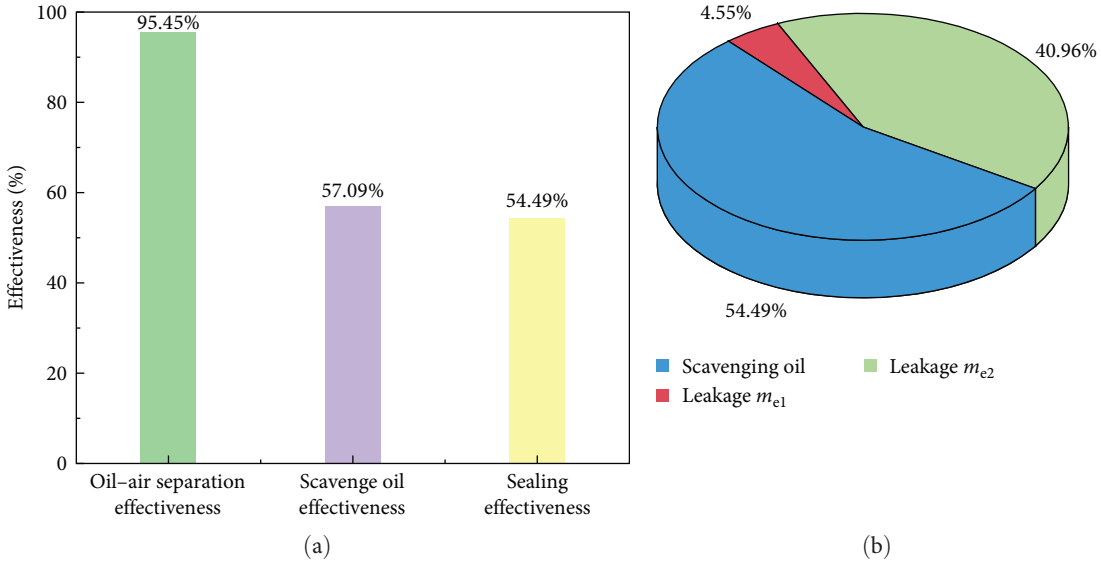

Figure 7: Sealing effectiveness and lubricating oil distribution of seal system: (a) the sealing effectiveness of seal system; (b) the lubricating oil distribution of seal system.

separation effectiveness of each seal chamber corresponding to different depth–width ratios of the stator chamber. With the increase of the depth–width ratio of the stator chamber, the oil–air separation effectiveness of the chamber *I* and *III* first increases and then decreases, the oil–air separation effectiveness of the chamber *II* first decreases and then increases, and the amount of lubricating oil separated in the chamber *III* first increases and then decreases. The lubricating oil accumulated in chamber *III* is more likely to leak from the outlet along the radial seal, which makes the η_{sca} decrease first and then increase.

The movement of the mixture medium in the seal system is influenced by the structure of the rotor chamber, which alters the incidence angle and velocity of oil droplets entering

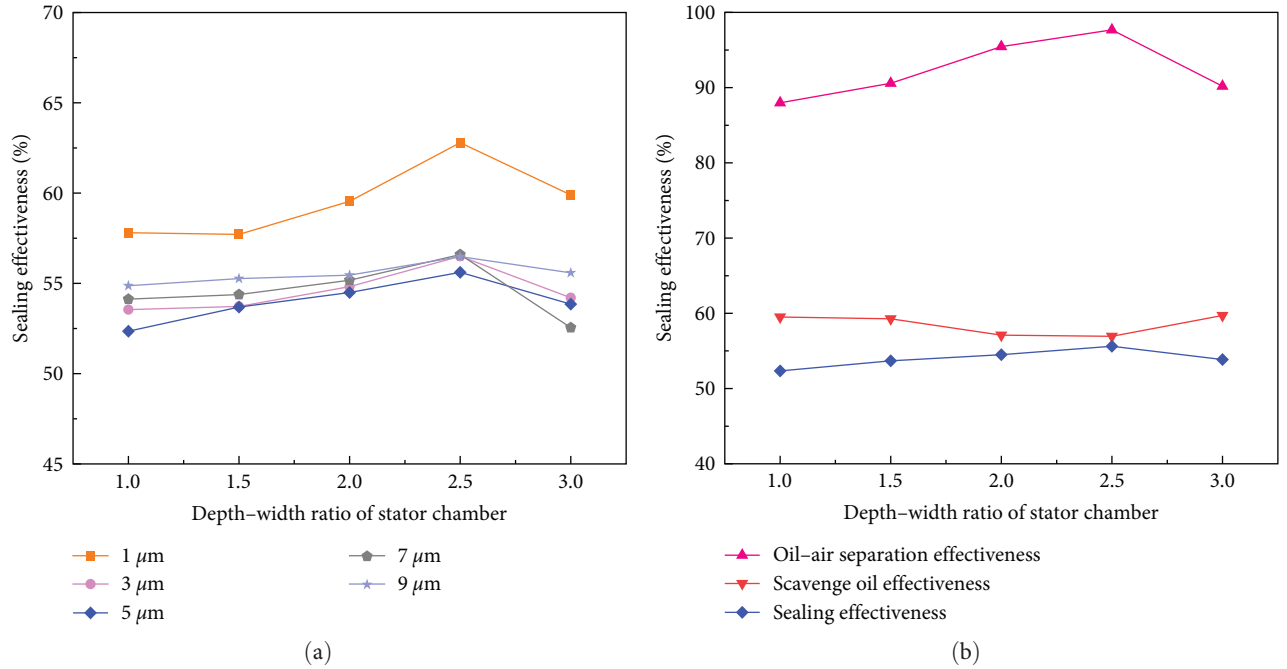

FIGURE 8: The relation between the depth–width ratio of stator chamber and η_{seal}: (a) oil droplets with different diameters; (b) oil droplets with medium diameter.

the stator chamber, leading to different η_{sep} and accumulated lubricating oil among the chambers. The η_{seal} for different oil droplet diameters is depicted in Figure 11(a), which shows a decreasing and then increasing trend as the depth–width ratio of the rotor chamber decreases. To further analyze this trend, Figure 11(b) illustrates the impact of rotor chamber depth–width ratio on η_{sep}, η_{sca}, and η_{seal} of medium-diameter oil droplets. As the depth–width ratio of the rotor chamber goes down, the η_{sep} goes down, the η_{sca} goes up, and the η_{seal} goes down first, then up by the two effects work together.

The wall surface of the rotor chamber rotates at high speed, and its internal flow field is more complex than that of the stator chamber. Changing the structural parameters of the chamber will change the trajectory of the oil droplets and affect the separation effectiveness of each seal chamber. As shown in Figure 12, as the depth–width ratio of the rotor chamber gradually decreases, the complete vortex inside the rotor chamber will be destroyed, the centrifugal force on the oil droplets will be weakened, and the drag effect of the direct airflow will be dominated. Therefore, oil droplets are more likely to pass directly through the axial seal clearance without colliding with the wall, and the η_{sep} has been reduced. The high-speed rotation of the rotor chamber generates strong centrifugal force on the lubricating oil adhering to the wall surface of the rotor chamber, causing them to enter the stator chamber and achieve effective reflux. Reducing the depth–width ratio of the rotor chamber will increase the centrifugal force acting on the lubricating oil, making it easier for separated lubricating oil to flow back effectively, resulting in a significant improvement in η_{sca}. The η_{seal} exhibits a nonmonotonic trend, initially decreasing and then increasing, as a result of the combined influence of the η_{sep} and η_{sca}.

5.3. Influence of Axial Seal Clearance. The clearance width of the axial seal determines the flow rate of the oil–air mixture medium entering the seal chamber, thereby affecting the distribution of the internal flow field and the trajectory of the oil droplets, which ultimately affects the η_{seal} and m_e. In Figure 13(a), the relationship between the width of the axial seal clearance and the η_{seal} for oil droplets of different diameters is shown. It is observed that as the axial seal clearance width widens, the η_{seal} decreases. Figure 13(b) shows the relationship between the axial clearance width and the η_{sep}, η_{sca}, and η_{seal} for medium-diameter oil droplets. As the axial clearance width widens, the η_{sep} and η_{sca} decrease, leading to a reduction in η_{seal}.

As the axial seal clearance widens, the straight-through effect of the airflow is enhanced, making it easier for oil droplets to be entrained by the airflow and pass through the seal chamber without colliding with the wall surface, as shown in Figure 14. This reduces the η_{sep} and increases m_{e1}. As the straight-through effect of the seal system is enhanced, oil droplets from chambers *I* and *II* are more likely to enter chamber *III*. However, due to the radial seal set at the tail of the seal system, the oil–air separation effectiveness of chamber *III* is increased, leading to an increased accumulation of lubricating oil in chamber *III*. Under the pressure difference between the seal chamber and the outlet, the lubricating oil accumulated in chamber *III* is more likely to leak from the outlet along the radial seal, resulting in a decrease in η_{sca} and an increase in m_{e2}. Therefore, an increase in axial seal clearance width leads to a decrease in η_{sep} and η_{sca}, ultimately reducing the η_{seal}. To avoid insufficient seal clearance caused by thermal expansion and wear of seal teeth, it is important to ensure a small axial seal clearance width in seal system

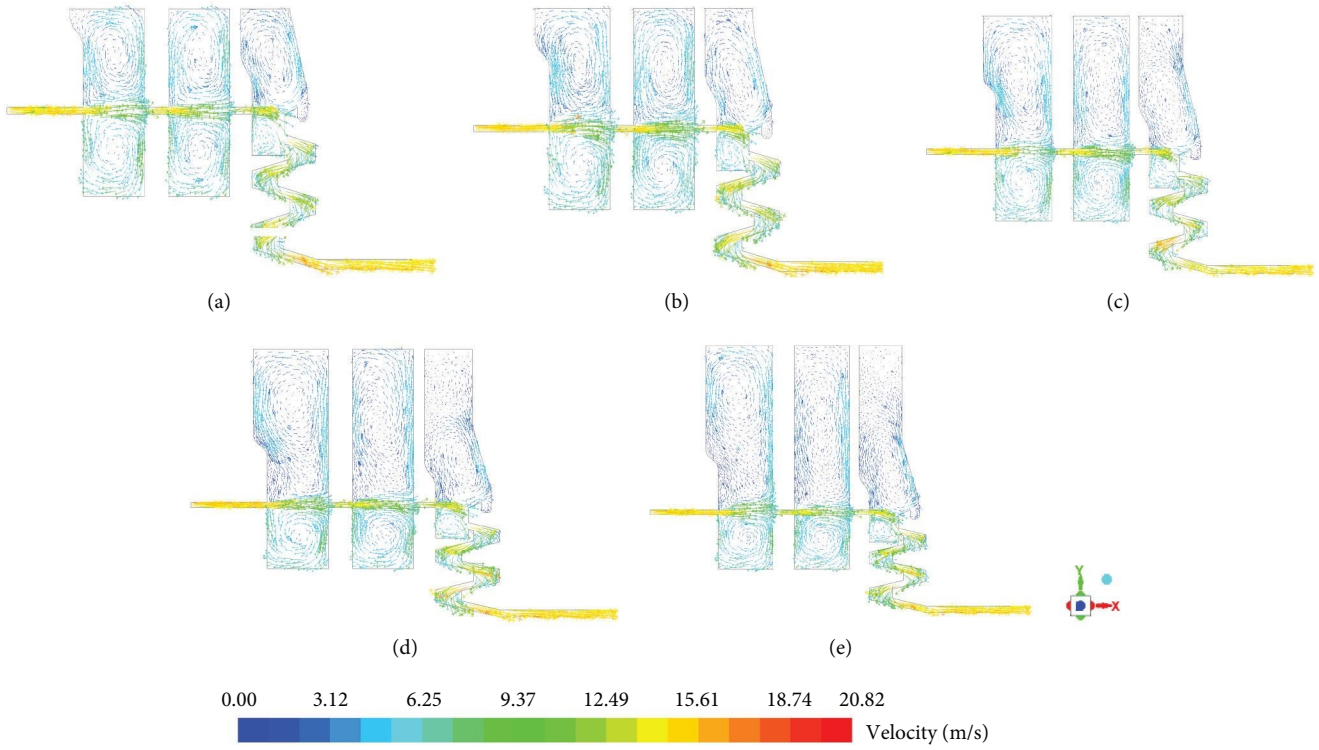

Figure 9: The velocity vector diagram of seal system with different depth–width ratios of stator chamber: (a) the depth–width ratio of stator chamber is 1.0; (b) the depth–width ratio of stator chamber is 1.5; (c) the depth–width ratio of stator chamber is 2.0; (d) the depth–width ratio of stator chamber is 2.5; (e) the depth–width ratio of stator chamber is 3.0.

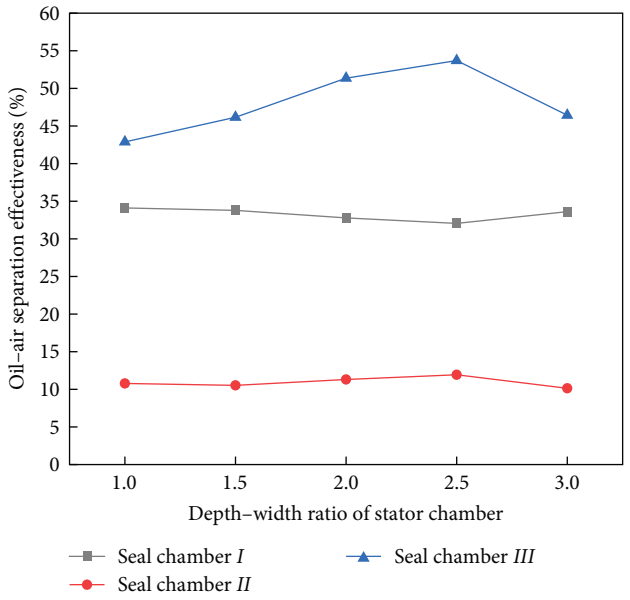

Figure 10: The relation between the depth–width ratio of stator chamber and η_{sep}.

design and consider the influence of temperature-induced expansion and deformation of seal teeth on seal clearance [21].

The variation in the relative height of the axial seal clearance alters the flow path of the oil–air mixture, leading to changes in oil droplet trajectories and, in turn, affects the η_{sep}, η_{sca}, and η_{seal}. Figure 15(a) illustrates the relationship between radial seal height difference and η_{seal} for oil droplets with different diameters, while Figure 15(b) displays the correlation between radial seal height difference and η_{sep}, η_{sca}, and η_{seal} for 5 μm diameter oil droplets. The lowest η_{seal} of the seal system occurs when the axial clearance height is 0. A larger radial height difference leads to an increase in η_{sep} and η_{sca}, thereby enhancing the η_{seal}.

When the axial clearance height is zero, the seal system exhibits a significant straight-through effect, as shown in Figure 16(c). At this point, the oil droplets are more easily entrained by the airflow and directly pass through seal chambers *I* and *II* to reach chamber *III*. Therefore, the separation effectiveness of seal chamber *III* is higher, and more lubricating oil accumulates in this chamber, which is more likely to leak from the outlet, resulting in the lowest η_{sca}. When the seal clearance moves toward the rotor chamber, it weakens the straight-through effect and enhances the eddy current intensity in the rotor chamber, as shown in Figures 16(a) and 16(b). In contrast, when the seal clearance moves toward the stator chamber, the vortex in the stator chamber will be strengthened, as shown in Figures 16(d) and 16(e).

Whether the seal clearance moves toward the rotor chamber or stator chamber, it will weaken the straight-through effect and increase the centrifugal force on the oil droplets. Therefore, more oil droplets will be separated by chambers *I* and *II*, reducing the accumulation of lubricating oil in seal chamber *III*, which will significantly improve the

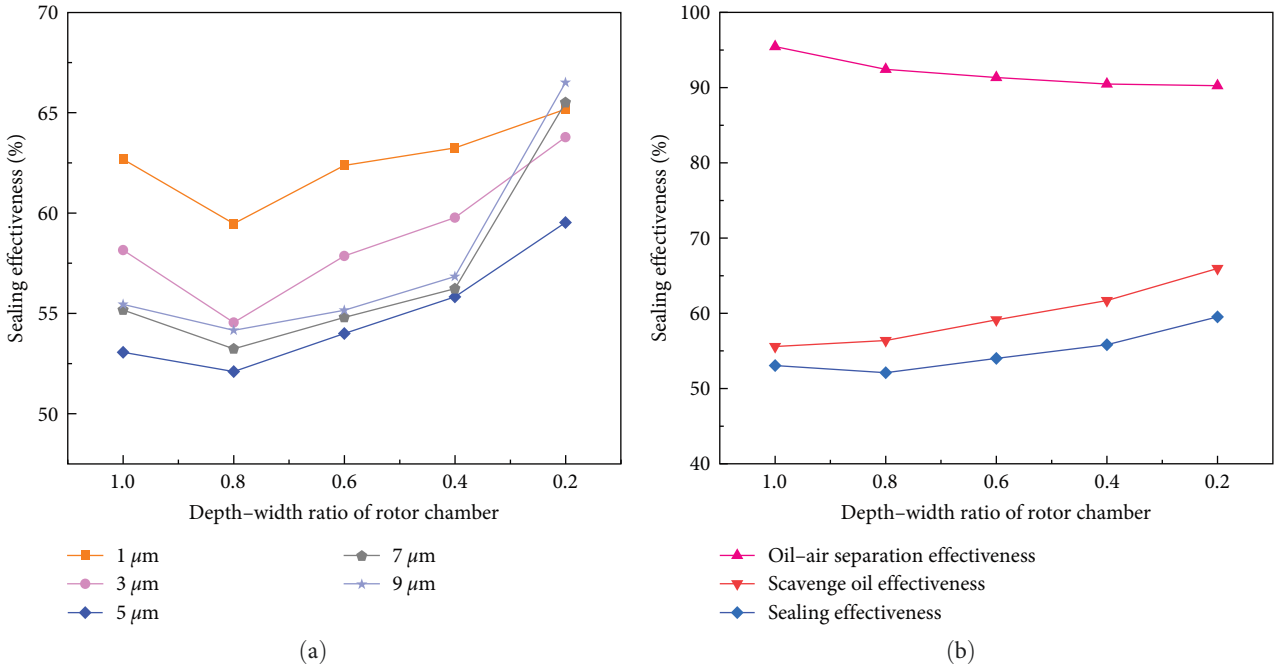

FIGURE 11: The relation between the depth–width ratio of rotor chamber and η_{seal}: (a) oil droplets with different diameters; (b) oil droplets with medium diameter.

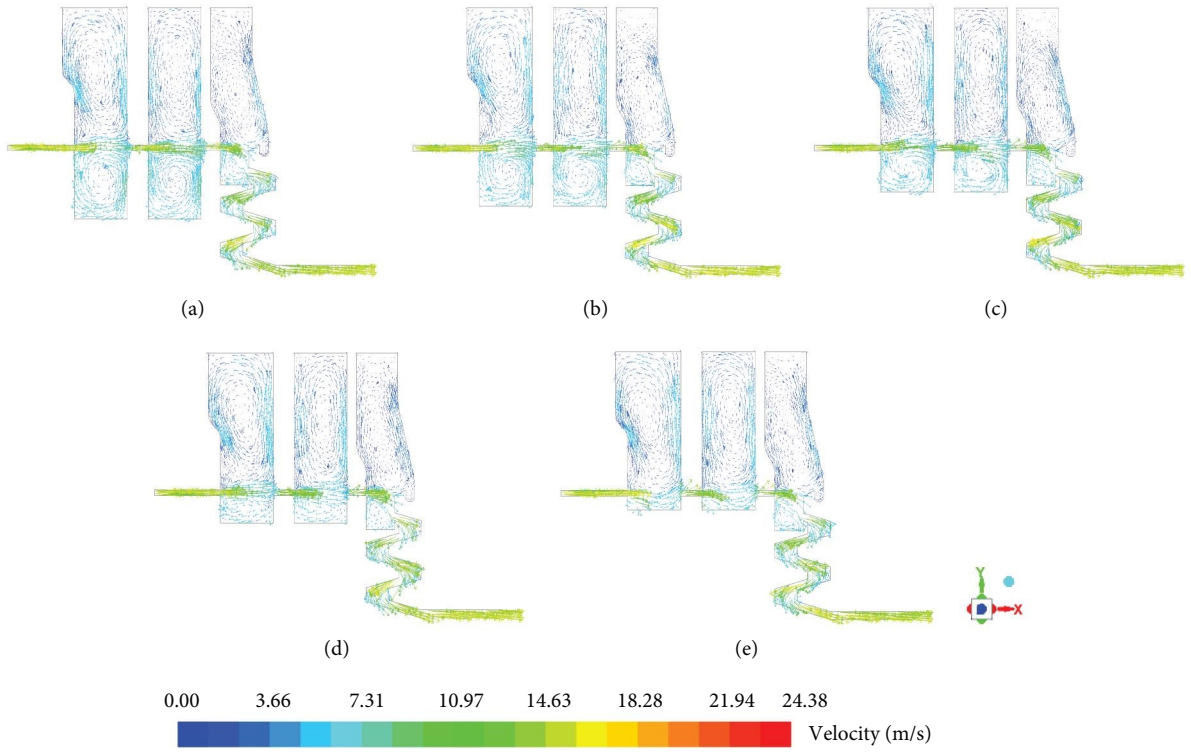

FIGURE 12: The velocity vector diagram of seal system with different depth–width ratios of rotor chamber: (a) the depth–width ratio of rotor chamber is 1.0; (b) the depth–width ratio of rotor chamber is 0.8; (c) the depth–width ratio of rotor chamber is 0.6; (d) the depth–width ratio of rotor chamber is 0.4; (e) the depth–width ratio of rotor chamber is 0.2.

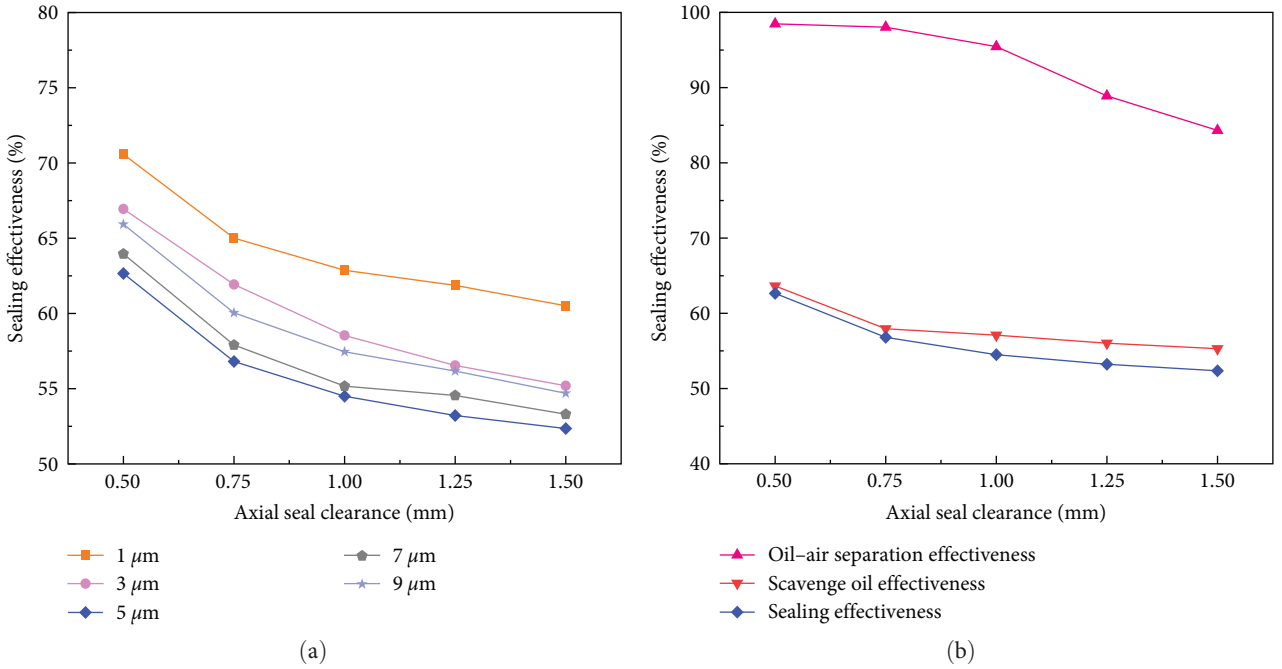

FIGURE 13: The relation between the axial seal clearance width and η_{seal}: (a) oil droplets with different diameters; (b) oil droplets with medium diameter.

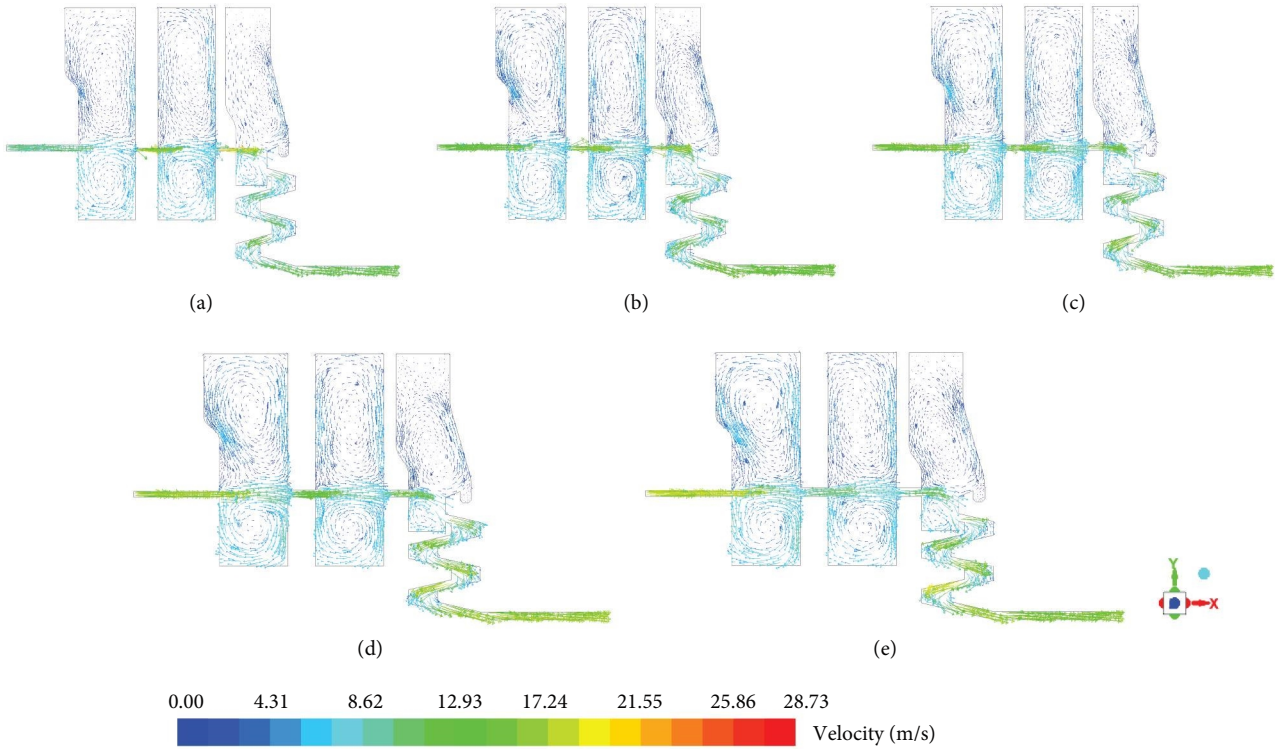

FIGURE 14: The velocity vector diagram of seal system with different axial seal clearance: (a) the axial seal clearance is 0.5 mm; (b) the axial seal clearance is 0.75 mm; (c) the axial seal clearance is 1.00 mm; (d) the axial seal clearance is 1.25 mm; (e) the axial seal clearance is 1.50 mm.

η_{sca}. In addition, when the seal clearance moves toward the stator chamber, it will increase the surface area of the rotor chamber wall. The oil droplets adhering to seal chamber walls are easier to achieve scavenge oil, and the η_{sca} is higher.

5.4. Influence of Scavenge Oil Structure. The scavenge oil structure of the seal system not only impacts scavenge oil performance but also affects the pressure distribution in each seal chamber. As a result, the trajectory of oil droplets and

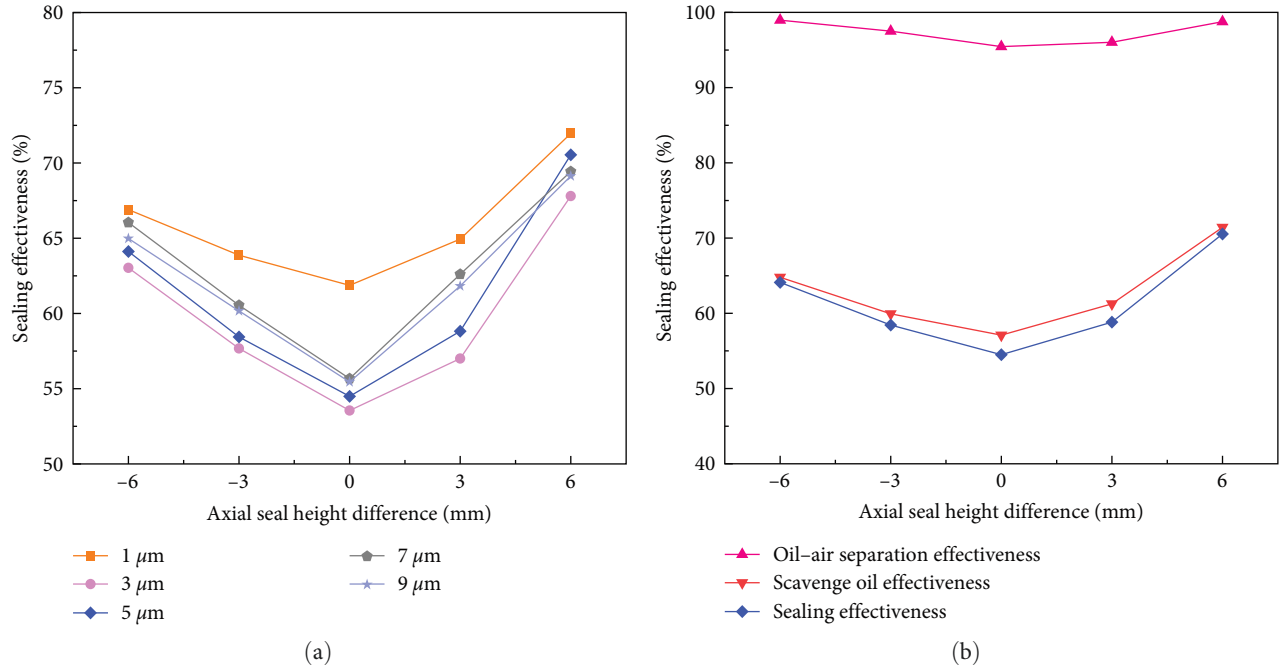

Figure 15: The relation between the axial seal height difference and η_{seal}: (a) oil droplets with different diameters; (b) oil droplets with medium diameter.

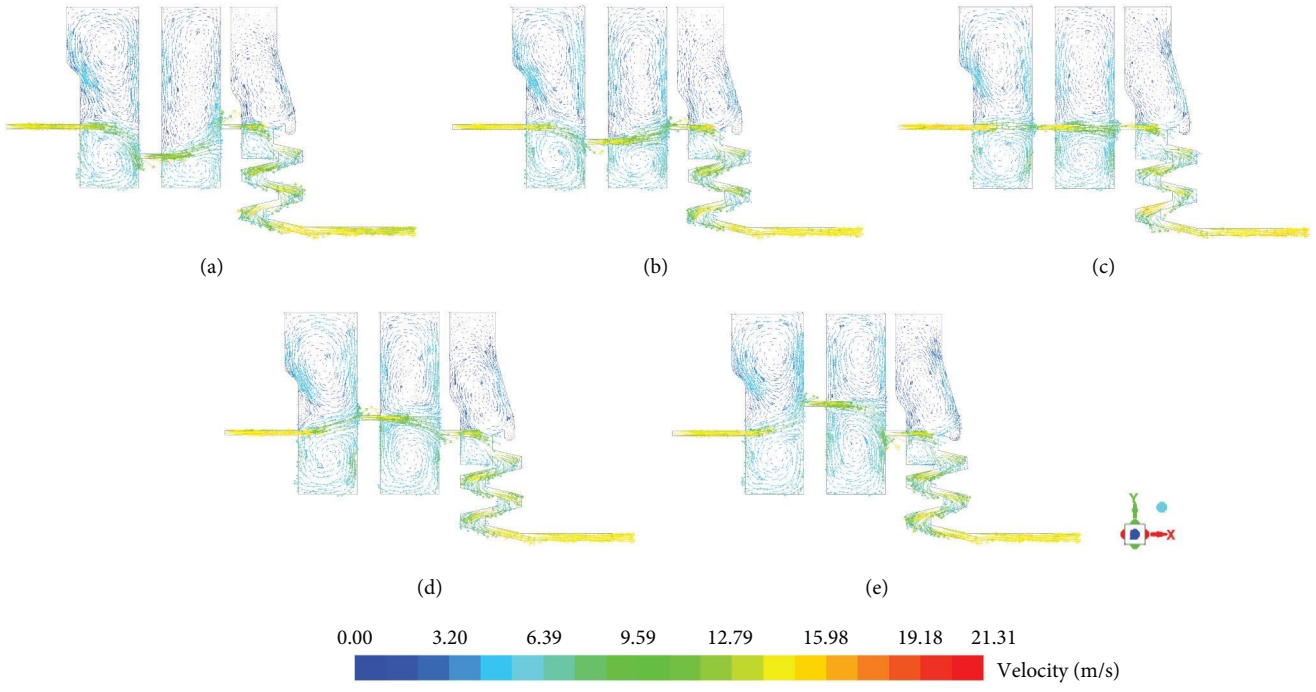

Figure 16: The velocity vector diagram of seal system with different axial seal height differences: (a) the axial seal height difference is −6 mm; (b) the axial seal height difference is −3 mm; (c) the axial seal height difference is 0 mm; (d) the axial seal height difference is 3 mm; (e) the axial seal height difference is 6 mm.

the η_{sep} are influenced. Figures 17(a) and 18(a) give the relationship curves between the diameter of the primary scavenge oil hole, the diameter of the secondary scavenge oil hole, and the η_{seal}, respectively. The medium-diameter oil droplets are selected to analyze the influence of the diameter of the primary scavenge oil hole and the diameter of the secondary scavenge oil hole on the η_{sep} and η_{sca}, as illustrated in Figures 17(b) and 18(b). It is possible to see that as the

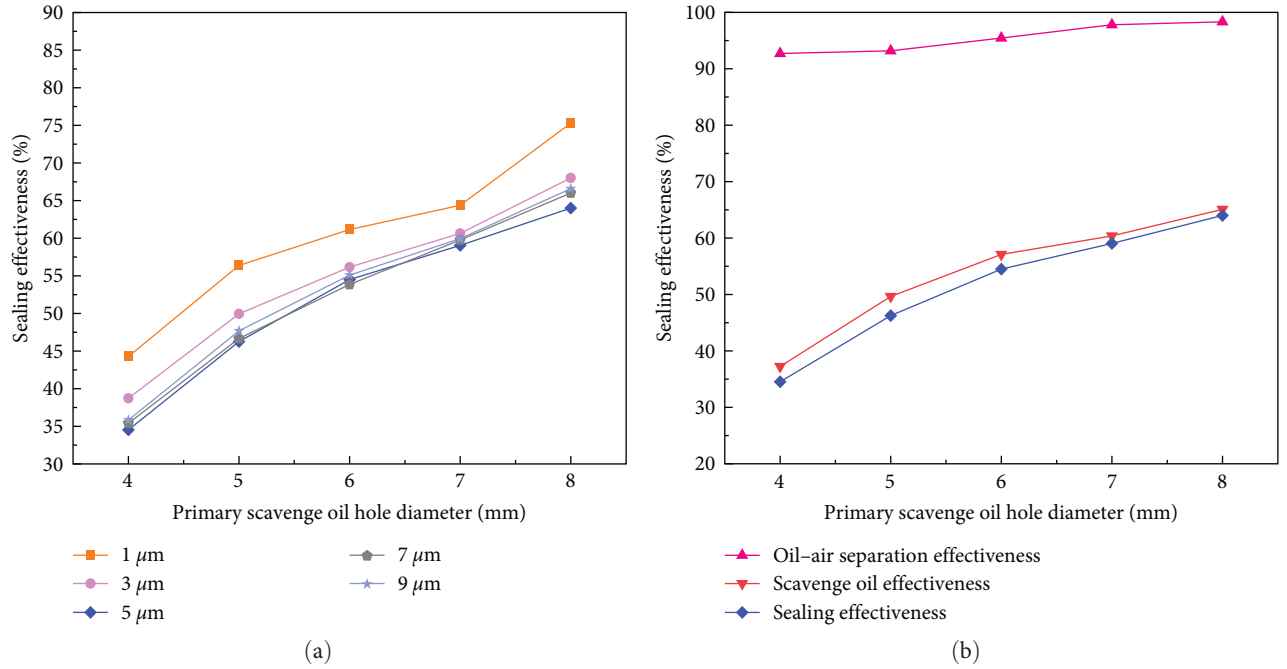

FIGURE 17: The relation between the primary scavenge oil hole diameter and η_{seal}: (a) oil droplets with different diameters; (b) oil droplets with medium diameter.

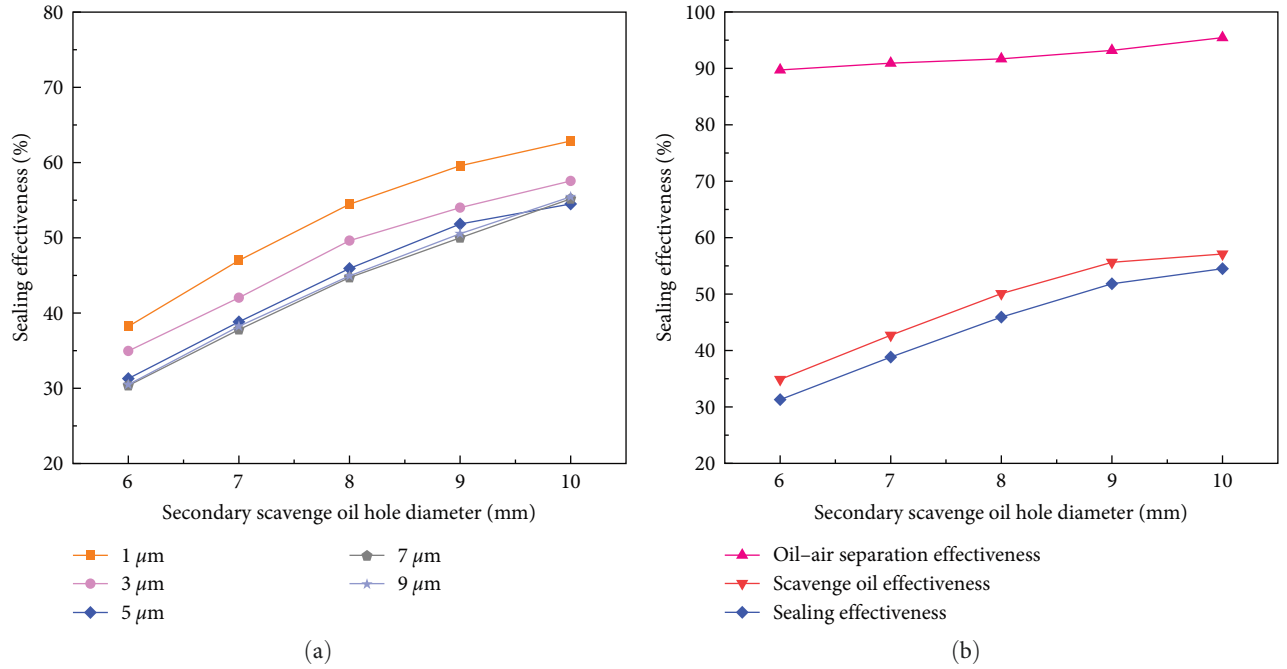

FIGURE 18: The relation between the secondary scavenge oil hole diameter and η_{seal}: (a) oil droplets with different diameters; (b) oil droplets with medium diameter.

diameters of the primary and secondary scavenge oil holes increase, the η_{sep} and η_{sca} are improved, which improves the η_{seal}.

Expanding the diameter of the scavenge oil hole helps to improve the flowability of the oil–air mixture between the labyrinth seal and the scavenge oil port, as shown in Figures 19 and 20. Driven by the pressure difference between the labyrinth seal and the scavenge oil port, the mixed medium flows from the high-pressure side of the labyrinth seal to the low-pressure side of the scavenge oil port. Some lubricating oil droplets are entrained by the airflow and flow directly back to the gearbox through the scavenge oil port. Expanding the diameter of the scavenge oil hole increases the surface area of the scavenge oil structure, which also

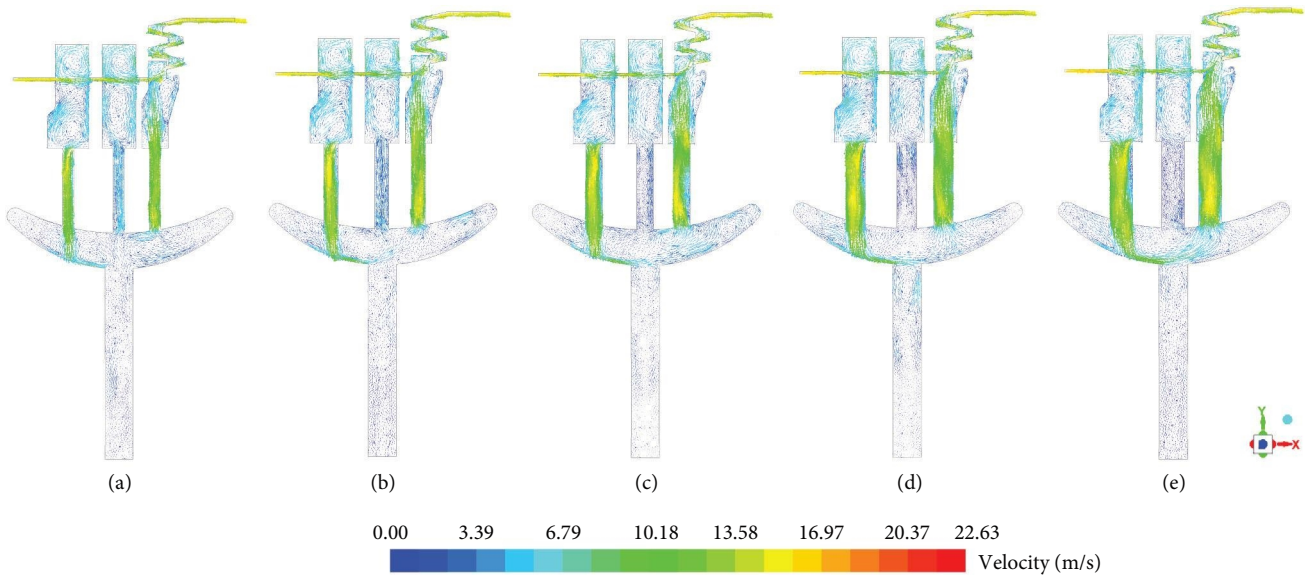

Figure 19: The velocity vector diagram of seal system with different primary scavenge oil hole diameter: (a) the primary scavenge oil hole diameter is 4 mm; (b) the primary scavenge oil hole diameter is 5 mm; (c) the primary scavenge oil hole diameter is 6 mm; (d) the primary scavenge oil hole diameter is 7 mm; (e) the primary scavenge oil hole diameter is 8 mm.

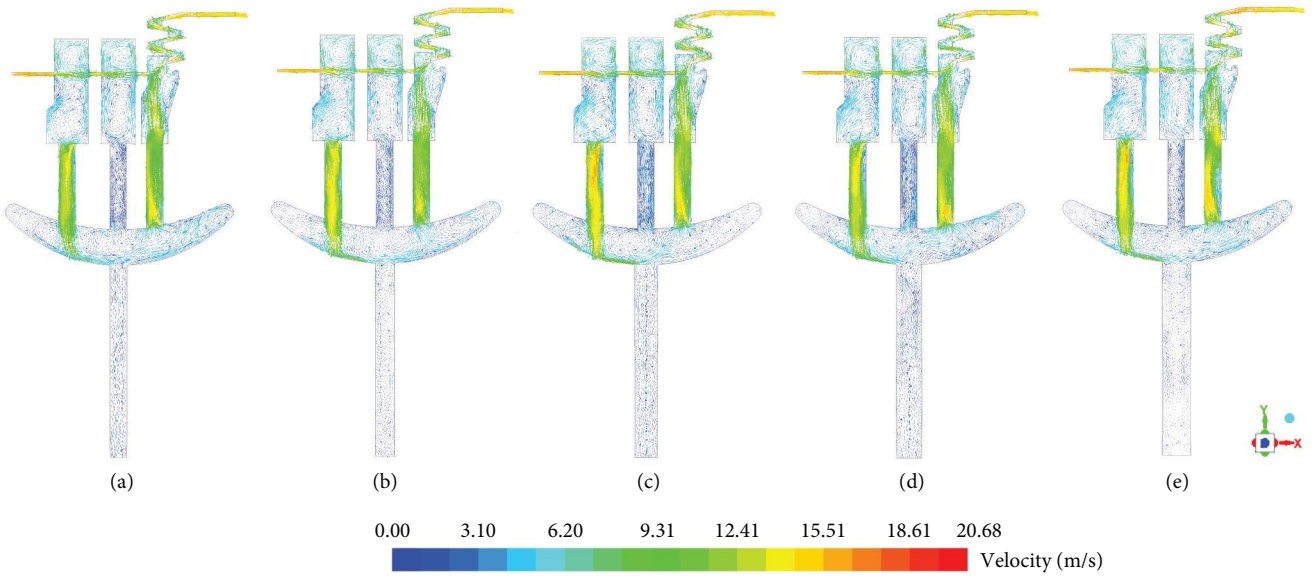

Figure 20: The velocity vector diagram of seal system with different secondary scavenge oil hole diameter: (a) the secondary scavenge oil hole diameter is 6 mm; (b) the secondary scavenge oil hole diameter is 7 mm; (c) the secondary scavenge oil hole diameter is 8 mm; (d) the secondary scavenge oil hole diameter is 9 mm; (e) the secondary scavenge oil hole diameter is 10 mm.

facilitates collision and separation of oil droplets, improving the η_{sep}. In addition, expanding the diameter of the scavenge oil hole significantly enhances the reflux characteristics of the separated lubricating oil, improving the η_{sca}.

As the diameter of the scavenge oil hole raises, the η_{sep} is slightly increased, and the η_{sca} is significantly improved, resulting in a considerable improvement in the η_{seal} and a significant reduction in m_e. Due to the larger number of primary scavenge oil holes and the presence of a collection and buffer structure at the bottom, in comparison, the secondary scavenge oil holes are fewer. Therefore, increasing the diameter of the primary scavenge oil holes will significantly improve η_{seal}. Consequently, in the structural design of a gearbox seal system, selecting a larger diameter for the scavenge oil hole, if space permits, is conducive to improving the seal system's performance and reducing leakage.

6. Conclusions

The sealing effectiveness of seal system η_{seal} relies on the effectiveness of oil–air separation of the seal system η_{sep} and the effectiveness of scavenge oil of the seal system η_{sca}.

To determine the optimal size parameters during the design process, an analysis of the seal system performance was conducted through the perspective of oil–air separation and scavenge oil. The study investigated the influence of the seal chamber depth–width ratio, axial seal clearance width and height difference, and scavenge oil hole diameter on the seal effectiveness. Based on the analysis, the following conclusions can be drawn:

(1) The η_{sep} is influenced by the drag effect of straight-through airflow and the centrifugal effect of the vortex. The stronger the drag effect of straight-through airflow or the weaker the centrifugal effect of the vortex, the lower the η_{sep}, and the lower the m_{e1}.

(2) The η_{sca} is related to the separation effectiveness of each seal chamber. The higher the oil–air separation effectiveness of chamber *I*, the lower the separation effectiveness of chamber *III*, the higher the η_{sca} and the less m_{e2}.

(3) The seal system studied in this paper achieves optimal sealing effectiveness with a stator chamber depth–width ratio of 2.5, but effectiveness is the lowest when the depth–width ratio of the rotor chamber is 0.2. Increasing axial seal clearance reduces system sealing effectiveness. When the axial seal clearance width is increased from 0.5 to 1.5 mm, the η_{seal} decreases by about 10%. Axial seal clearance height difference improves the η_{seal}. Moving axial seal clearance toward the stator chamber by 3 mm increases η_{seal} by about 3%, while moving toward the rotor chamber by 3 mm results in an increase of about 5%. Moving axial seal clearance toward the stator chamber by 6 mm increases η_{seal} by about 9%, while moving toward the rotor chamber by 6 mm results in an increase of about 13% in η_{seal}.

(4) By increasing the diameter of the scavenge oil holes, the seal performance of the seal system can be improved. Moreover, for the improvement of seal performance in the seal system, increasing the diameter of the primary scavenge oil holes has a more significant effect. The diameter of the primary scavenge oil holes has been increased from 4 to 8 mm, resulting in an approximate 30% improvement in η_{seal}. Similarly, the diameter of the secondary scavenge oil holes has been increased from 6 to 10 mm, resulting in an approximate 24% improvement in η_{seal}.

In summary, the seal performance of the gearbox seal system depends on both oil–air separation performance and scavenge oil performance. In order to achieve an optimized seal system, it is important to take into account the depth–width ratio of the stator chamber, axial seal clearance width and height difference, scavenge oil hole diameter, and the separation effectiveness of each seal chamber. By selecting appropriate parameters, the oil–air separation and scavenge oil performance of the seal system can be improved, resulting in better overall seal performance.

Nomenclature

t: Time
u: Velocity
Γ_ϕ: Diffusion coefficient
S_ϕ: Source term
F_D: Drag force per unit discrete phase mass
u_c: Continuous phase velocity
u_d: Discrete phase velocity
μ_c: Continuous phase hydrodynamic viscosity
ρ_c: Continuous phase density
ρ_d: Discrete phase density
d_p: Discrete phase diameter
C_D: Drag coefficient
Re_d: Discrete phase Reynolds number
g: Acceleration of gravity
F_x: Additional force on a single particle
α_q: Volume fraction of the qth phase
v_q: Velocity of the qth phase
$S\alpha_q$: Source term of the qth phase
ρ_q: Density of the qth phase
α_{air}: Volume fraction of air
α_{oil}: Volume fraction of lubricating oil
ρ_o: Oil droplet density
d_o: Oil droplet diameter
μ_o: Oil droplet viscosity
σ_o: Oil droplet surface tension
V_n: Normal collision velocity of the oil droplet
We: Weber number
La: Laplace number
k: Turbulent kinetic energy
i, j: Tensor indexes
x: Displacement
a_k: Reciprocal of the effective turbulent Prandtl number of turbulent kinetic energy
a_ε: Reciprocal of the effective turbulent Prandtl number of turbulent dissipation rate
μ_{eff}: Correction term of turbulence model to turbulent viscosity
$C_{1\varepsilon}^*$: Correction coefficient of RNG k–ε turbulence model constant $C_{1\varepsilon}$
$C_{1\varepsilon}$, $C_{2\varepsilon^*}$: RNG k–ε turbulence model constant
e_n: Normal rebound coefficient
e_τ: Tangential rebound coefficient
m_e: Quality of lubricating oil that leaks from the gearbox seal system
m_{e1}: Lubricating oil quality that leaked without oil–air separation
m_{e2}: Lubricating oil quality that achieved oil–air separation but lacked adequate scavenging oil
η_{sep}: Effectiveness of oil–air separation of the seal system
m_{in}: Total mass of oil droplets that enter the seal system
η_{sca}: Effectiveness of scavenge oil of the seal system
η_{seal}: Sealing effectiveness of seal system
m_1: Oil that is not separated is collected by oil–gas collection tooling *I*

m_2: Separated oil is collected by oil–gas collection tooling *II*

Greek Symbols

ϕ: General variable
ρ: Fluid density
ε: Dissipation rate
η: Separation effectiveness of oil–gas separator
θ: Angle of incidence

Subscripts

sep: Separation
sca: Scavenge
seal: Seal

Abbreviations

EMU: Electrical multiple units
VOF: Volume of fluid
DPM: Discrete phase model
RNG: Renormalization group.

Data Availability

The data that support the findings of this study are available from the corresponding author upon reasonable request.

Conflicts of Interest

The authors declare that they have no conflicts of interest.

Acknowledgments

This research was funded by the National Natural Science Foundation of China (U2268211), the National Natural Science Foundation of Sichuan Province (2022NSFSC0034 and 2022NSFSC1901), the Independent Research and Development Projects of State Key Laboratory of Heavy Duty AC Drive Electric Locomotive Systems Integration (R111720H01385) and the Independent Research and Development Projects of State Key Laboratory of Traction Power (2022TPL-T02).

References

[1] Y. Zhang, J. Li, D. Ma et al., "Experimental and numerical investigations on the leakage flow characteristics of helical-labyrinth-brush seals," *Journal of Engineering for Gas Turbines and Power*, vol. 143, no. 4, Article ID 041023, 2021.

[2] M. Zhang, J. Yang, W. Xu, and Y. Xia, "Leakage and rotordynamic performance of a mixed labyrinth seal compared with that of a staggered labyrinth seal," *Journal of Mechanical Science and Technology*, vol. 31, pp. 2261–2277, 2017.

[3] T. Wu and L. San Andrés, "Leakage and dynamic force coefficients for two labyrinth gas seals: teeth-on-stator and interlocking teeth configurations. A computational fluid dynamics approach to their performance," *Journal of Engineering for Gas Turbines and Power*, vol. 141, no. 4, Article ID 042501, 2019.

[4] L. S. Andrés, T. Wu, J. Barajas-Rivera, J. Zhang, and R. Kawashita, "Leakage and cavity pressures in an interlocking labyrinth gas seal: measurements versus predictions," *Journal of Engineering for Gas Turbines and Power*, vol. 141, no. 10, Article ID 101007, 2019.

[5] X. Yan, X. Dai, K. Zhang, J. Li, and K. He, "Effect of teeth bending and mushrooming damages on leakage performance of a labyrinth seal," *Journal of Mechanical Science and Technology*, vol. 32, pp. 4697–4709, 2018.

[6] A. H. Haghiabi, M. R. Ghaleh Nou, and A. Parsaie, "The energy dissipation of flow over the labyrinth weirs," *Alexandria Engineering Journal*, vol. 61, no. 5, pp. 3729–3733, 2022.

[7] N. Wang, Y. Wang, and A. Tian, "Influence of structure parameters on aeroelastic stability for labyrinth seal based on energy method," *Propulsion and Power Research*, vol. 7, no. 4, pp. 288–295, 2018.

[8] W. D. He, C. Wang, and Y. H. Zhang, "Study of the influence of labyrinth seal clearance on gearbox leakage with gas-fluid two-phase mixture," *Applied Mechanics and Materials*, vol. 789-790, pp. 231–235, 2015.

[9] M. Zhang and D. W. Childs, "Effects of increased tooth clearance on the performance of a labyrinth seal with oil-rich bubbly laminar flow," *Journal of Engineering for Gas Turbines and Power*, vol. 143, no. 11, Article ID 111007, 2021.

[10] Z. Li, Z. Fang, and J. Li, "Numerical investigation on the leakage and rotordynamic characteristics for three types of annular gas seals in wet gas conditions," *Journal of Engineering for Gas Turbines and Power*, vol. 141, no. 3, Article ID 032504, 2019.

[11] M. Farrall, K. Simmons, S. Hibberd, and P. Gorse, "A numerical model for oil film flow in an aeroengine bearing chamber and comparison to experimental data," *Journal of Engineering for Gas Turbines and Power*, vol. 128, no. 1, pp. 111–117, 2006.

[12] M. Farrall, S. Hibberd, K. Simmons, and D. Giddings, "Prediction of air/oil exit flows in a commercial aero-engine bearing chamber," *Proceedings of the Institution of Mechanical Engineers, Part G: Journal of Aerospace Engineering*, vol. 220, no. 3, pp. 197–202, 2006.

[13] Y. Zhang, K.-L. Zhang, and Y. Yao, "Effect of seal clearance on the separation performance for a gearbox sealing system of a high-speed electric multiple unit," *Journal of Zhejiang University-SCIENCE A*, vol. 20, pp. 358–367, 2019.

[14] Y. Zhang, K. Zhang, and Y. Yao, "Study on oil-gas separation characteristics of gearbox seal system of high-speed electric multiple unit," *Computing in Science & Engineering*, 2019.

[15] H.-N. Tang, S.-J. Wang, and J. Zhao, "Effect of fluid-structure interaction on sealed flow field and leakage rate based on computational fluid dynamics," *Journal of Shanghai Jiaotong University (Science)*, vol. 20, pp. 326–330, 2015.

[16] X. Gao, J. Chen, J. Feng, and X. Peng, "Numerical and experimental investigations of the effects of the breakup of oil droplets on the performance of oil–gas cyclone separators in oil-injected compressor systems," *International Journal of Refrigeration*, vol. 36, no. 7, pp. 1894–1904, 2013.

[17] C. Bai and A. D. Gosman, "Development of methodology for spray impingement simulation," *SAE Transactions*, vol. 104, pp. 550–568, 1995.

[18] Q. Peng, L. Gui, and Z. Fan, "Numerical and experimental investigation of splashing oil flow in a hypoid gearbox," *Engineering Applications of Computational Fluid Mechanics*, vol. 12, no. 1, pp. 324–333, 2018.

[19] G. Grant and W. Tabakoff, "Erosion prediction in turbomachinery resulting from environmental solid particles," *Journal of Aircraft*, vol. 12, no. 5, pp. 471–478, 1975.
[20] Y. Lu, "*Gas engine labyrinth oil gas separation numerical simulation research*," M.S. thesis, Guangxi University, Nanning, Guangxi, China, 2016.
[21] Y. Zhang, K.-L. Zhang, and Y. Yao, "Impact of rotating and thermal effects on leakage performance of gearbox with axial labyrinth seal," *Journal of Zhejiang University (Engineering Science)*, vol. 53, no. 9, pp. 1656–1662, 2019.